Eng. Sci., 2022, **20**, 162–179

Engineered Science

DOI: https://dx.doi.org/10.30919/es8d757

Kinetic Modeling of the Pyrolysis of Propylene Glycol

Christina Al Gemayel,[1] Edward Honein,[1] Ahmad El Hellani,[2, 4] Rola Salman,[2, 4] Najat A. Saliba,[2, 4] Alan Shihadeh[3, 4] and Joseph Zeaiter[1,*]

Abstract

A kinetic model was developed to predict product evolution during the thermal degradation of propylene glycol (PG) under N_2 atmosphere. Main aldehydes that form from PG pyrolysis are formaldehyde (FA), acetaldehyde (AA), propanal (PA), acetone (Ace), glyoxal (GA) and methyglyoxal (MGA). Activation energies (Ea) of the proposed reaction pathways were determined experimentally under a range of temperatures via sequential parameter estimation and quasi-steady state approximation assumption. They were compared against Arrhenius parameters derived from ReaxFF-MD for aldehyde formation, with Ea errors between 3% for PA and up to 39% for Ace. ReaxFF-MD was also employed to assess reaction pathways and to compute Arrhenius parameters for PG cracking. PG decomposes at Ea=1.86E+05 J/mol and A_0=6.84E+13 s^{-1}. Model predictions were in agreement with experimental results and proved dehydration of PG to propylene oxide as the dominant pathway, which then undergoes ring opening to produce propen-1-ol and propen-2-ol. The two enols tautomerize to PA, Ace and FA—the major products from PG pyrolysis. Proposed elementary reactions were further studied on ReaxAMS to assess reaction pathways and transition states via the Nudged Elastic Band (NEB) method. This study's findings constitute a critical step in putting forward a comprehensive mathematical model for predicting toxicants in electronic cigarettes (ECIGS) emissions.

Keywords: Propylene glycol; Pyrolysis; electronic cigarette; Kinetic pathway; Computational chemistry.
Received: 05 June 2022; Revised: 11 June 2022; Accepted: 16 July 2022.
Article type: Research article

1. Introduction

Propylene glycol (PG) is a chemical commonly used in the food, cosmetics, and medical industries.[1] The thermal treatment of PG-containing matrix may yield decomposition reaction products.[2] Several studies have investigated the thermal decomposition of PG and highlighted the emission of toxic carbonyls.[3,4] In 2003, electronic cigarettes (ECIGS) were introduced to the market along with corresponding liquids in which PG is the main constituent.[5,6] The problem of thermal degradation of PG is particularly acute for ECIGs, which produce an inhalable aerosol by heating and vaporizing the liquid.[7] The inhalation exposure of ECIG users to the generated carbonyls has been a concern since the introduction of ECIGs into the market.[8-10] Predicting the amounts of toxicants yielded from a given process can help designers minimize their production, and this can be useful in minimizing carbonyl emissions from ECIGs.

The thermal degradation of PG under oxygen rich conditions at 400-500 K was shown to yield formaldehyde (FA), acetaldehyde (AA), and CO_2 via oxidative C-C bond cleavage.[11] The researchers suggested that PG follows a dehydration reaction to produce acetone (Ace). Ayre *et al.* (1994) investigated the adsorption and reaction of PG on oxygen activated Ag (110) surface, and they showed that PG adsorption occurred at 215 K, while degradation peaked at 340K to form acetol and lactaldehyde.[12] In 2012, Laino *et al.* reported the degradation mechanisms of PG by performing a pyrolysis study at 800K with 30 seconds of residence time.[3] Activation Gibbs free energy barriers and rate constants were calculated at this temperature. Salaev *et al.* (2016) performed a theoretical study of the gas phase oxidation of PG to methylglyoxal (MGA) over silver catalyst. It consisted of optimizing geometry parameters of gas-phase molecules, as

[1] *Baha and Walid Bassatne Department of Chemical and Petroleum Engineering, Maroun Semaan Faculty of Engineering and Architecture, American University of Beirut.*
[2] *Department of Chemistry, Faculty of Arts and Science, American University of Beirut.*
[3] *Department of Mechanical Engineering, Maroun Semaan Faculty of Engineering and Architecture, American University of Beirut.*
[4] *Center for the Study of Tobacco Products, Virginia Commonwealth University, Richmond, Virginia, USA.*
**Email:* jz08@aub.edu.lb (J. Zeaiter)

well as thermochemical data (heats of formation) for the stages of PG oxidation.[13]

In ECIG research, in an attempt to understand the mechanism of carbonyls generation, two ECIG device-independent pyrolysis studies were reported.[14,15] Wang *et al.* (2017) investigated the thermal degradation of five different ECIG liquids, including prepared mixtures of PG and vegetable glycerin, and commercially available liquids, in a stainless-steel tubular reactor.[14] They confirmed that the decomposition of PG and vegetable glycerin at temperatures above 450 K are the main sources of carbonyls in ECIGs: FA, AA, and acrolein were detected at different concentrations for various ECIG liquids. Our group reported a pyrolysis study of PG-saturated gas stream in a quartz tubular reactor at a wide range of temperatures (~350-940 K).[15] The influence of the atmosphere (air versus N_2), the temperature and the presence of coil material wires (nichrome, kanthal, stainless steel, and nickel) on the thermal degradation of PG was assessed.

Even though PG is not considered toxic for human health, its pyrolysis products, mainly FA (Formaldehyde), AA (Acetaldehyde) and PA (Propanal or propionaldehyde), are considered harmful.[3,16,17] In the 12th Report on Carcinogens conducted by National Toxicology Program, FA was classified as a known human carcinogen.[18] Acetaldehyde is classified as a Group B2 carcinogen by the United States Environmental Protection Agency (EPA), *i.e.*, it is a probable human carcinogen, as more human data is needed.[17] Finally, PA is linked to respiratory problems such as fluid build-up in lungs yet is not considered carcinogenic.[19]

Laino *et al.* studied the thermal decomposition mechanisms of PG by relying on simple decomposition based on dehydration of PG into either propylene oxide or allyl alcohol.[3] Propylene oxide can further decompose into acetone or propanal. They found energies such as total system energy, enthalpy and Gibbs free energy, theoretically from metadynamic simulations. The free energy surfaces found were optimized at the Density Functional Theory (DFT) level and the mechanism validated by GC-MS.

Herein, we present a kinetic model that relies on the data produced from the PG pyrolysis experiment in a quartz tube reactor under inert conditions.[15] By doing that, the thermal effect is isolated, and accurate parameters can be estimated for the thermal degradation process. The kinetic pathway mechanisms are determined based on the experimental data, and a rate-based kinetic model is developed. The activation energies for the reaction rate Arrhenius constants are calculated, under various temperatures that mimicked ECIG conditions, by employing sequential parameter estimation.[20] In addition, results are validated via quantum chemistry simulations. ReaxFF Molecular Dynamics (ReaxFF-MD), developed by van Duin *et al.*, is employed in this study, along with ReaxAMS, to predict reaction pathways, product formation, transition states, and energies. The importance of such atomistic-scale computational techniques has grown greatly over the years, mainly due to their accessibility and accuracy.[21] This study is critical to our efforts in putting forward a comprehensive mathematical model of toxicants in ECIG emissions.[22] Our works employs different perspectives: experiments, mathematical modeling, molecular dynamics, and elementary scale computations; it thus manages to merge these concepts into an unprecedented extensive study on PG pyrolysis.

2. Materials and methods

2.1 Experimental setup

We studied the homogeneous reaction of PG at various temperatures under inert conditions in a quartz tube reactor (Fig. 1). Controlled nitrogen gas flow (N_2) was passed through an impinger containing PG to generate a PG-saturated gas stream. A glass fiber filter was placed downstream of the impinger to intercept any mechanically-generated liquid particles. The 120 cm horizontal quartz tube reactor, with a radius of 0.33 cm, was placed in a two-zone rotary electric tube furnace (1200 °C max.). The 45 cm heated zone was nominally set at 100, 300, 400, 500, 600, or 700 °C. These temperatures corresponded to actual temperatures of 80, 256, 360, 460, 565, and 672 °C in the quartz tube reactor as measured using a K-type thermocouple. For each temperature condition, the mass flow through the reactor was adjusted to attain a fixed mean residence time of 1.6 s. Using the ideal gas law, the corresponding mass flow rates for the above temperatures were 386, 271, 236, 209, and 187 standard mL/min, respectively. The carbonyls in the outlet gas flow were trapped on DNPH-silica coated H10 cartridges, and then extracted with ethanol/acetonitrile (90/10) solution to be analyzed on HPLC. The detailed analytical method of carbonyl quantification is detailed elsewhere.[23] Six different carbonyls were detected and quantified: propionaldehyde (PA), acetone (Ace), acetaldehyde (AA), formaldehyde (FA), glyoxal (GA) and methylglyoxal (MGA).

2.2 Computational methods

2.2.1 Reactive Force Field ReaxFF-MD

Quantum mechanics (QM) is vastly used as a theoretical basis and a screening tool, as it is limited by its computational cost while working for larger systems (more than 100 atoms), and its inability to account for the dynamic progression of the system in question. QM calculations essentially solve the famous Schrodinger's equation:

$$\widehat{H\Psi}\left(r,\vec{t}\right) = ih\frac{\partial\Psi(\mathrm{r},\vec{t})}{\partial t} \quad (1)$$

which provides information on electron behavior and other events at the atomic scale. H is the Hamiltonian operator, which contains electron energies and other system details, and Ψ is the wave function which depends on electron position in space (r) and time ($\vec{t}$), and contains all physical properties of the system. QM is commonly used as a structure and energy basis for more advanced computations. Such calculations are referred to as empirical force fields (EFF), yielding interatomic potentials that compute, based on atom positions,

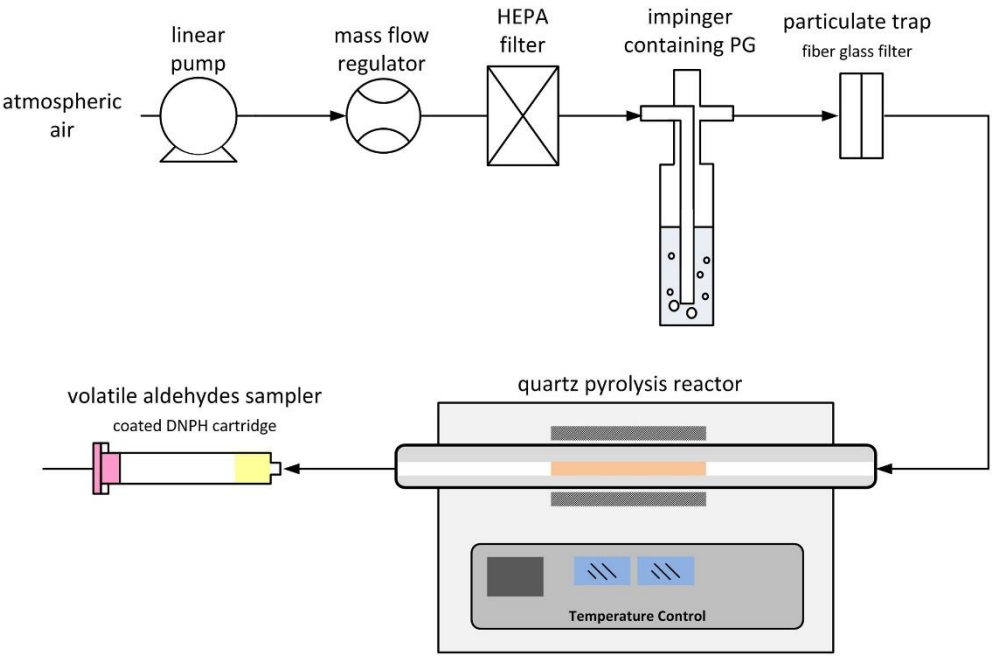

Fig. 1 Scheme for the pyrolysis reactor used in this study.[15]

the energy of the system. These potentials include harmonic potentials, van der Waals potentials and Coulombic interactions.[21] EFF are proven to work for large systems. EFF methods are accurate in describing non-reactive physical systems at or around equilibrium.[24] Hence, reactive force fields (ReaxFF) were introduced to expand such potentials to include a bond-order formalism, thus accounting for formation and breaking of bonds *i.e.*, chemical reactions. ReaxFF requires no pre-defined reaction mechanisms, proving to be an innovative tool that predicts system behavior based on environment-dependent reactive and non-reactive potentials, rather than user reaction input.

We employed the Amsterdam Modeling Suite's ReaxFF developed originally by Adri van Duin.[25] This package was provided by Software for Chemistry and Materials (SCM).[26] Originally developed for hydrocarbons, ReaxFF was later expanded for different systems. The general energy form in a ReaxFF simulation is computed as follows,

$$E_{system} = E_{bond} + E_{over} + E_{under} + E_{\mathrm{val}} + E_{\mathrm{pen}} + E_{\mathrm{tor}} + E_{conj} + E_{VdW} + E_{Coul} \quad (2)$$

where the system energy (E_{system}) is defined as a sum of energy terms.[27] Bond energy found from corrected bond order is defined as E_{bond}, with the two valence theory correction terms E_{over} and E_{under} to account for atom over-coordination and under-coordination, respectively. In addition, the valence angle energy is denoted by E_{val} in addition to the penalty energy (E_{pen}) term for systems sharing one atom in a valence angle while having double bonds. Furthermore, torsion angle energy (E_{tor}) and conjugation effects (E_{conj}), are accounted for. Finally, for non-bonded interactions, Van der Waals energy is accounted for in E_{VdW} term, and Coulomb interactions in E_{Coul}. Note that bond order is always updated as atomic positions are updated.[28] In this study, we investigated PG pyrolysis in ReaxFF, with the source code and Graphical User Interface (GUI) provided by SCM via AMS.[25]

2.2.2 Simulation details

A box of dimensions 23Å × 23Å × 23Å was filled with ten PG (1,2- Propanediol) molecules as illustrated in Fig. 2, via the 'Builder' option found in ReaxFF and provided by the Packmol package.[29] The distance between molecules was 2.5Å. Such volume and molecule number yield a density of 0.1038 g/cm^3, which was chosen based on preliminary trial-and-error simulations with other densities, where it provided better particle collisions leading to enhanced carbonyl formation, replicating the physical system of abundant PG input flow in e-cigarettes and in our experiment.

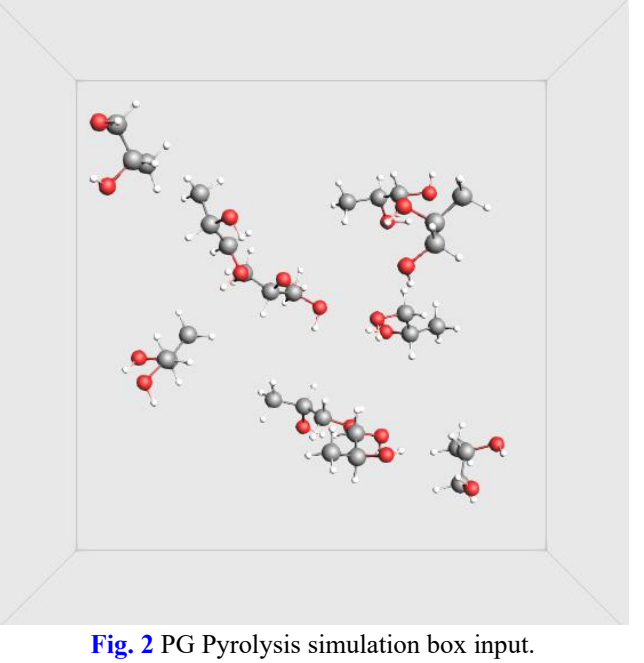

Fig. 2 PG Pyrolysis simulation box input.

After generating the reaction system, the CHO.ff: (C/H/O) hydrocarbon oxidation force field was chosen mainly since C, H and O are the only elements involved. This system was first subjected to a Number-Volume-Energy (NVE) microcanonical ensemble at 5K for 10ps in order to minimize its energy. Then the system was equilibrated for 10 ps isothermally at 1000K to ensure that all initial energies are constant with minimal fluctuations. It was set that no reaction takes place during these first 10 ps (equilibration stage). In this equilibration step, the Number-Volume-Temperature (NVT) canonical ensemble with a Berendsen thermostat was used to statistically describe the system; such ideal state is the most probable state for the real reaction system being simulated. The Berendsen thermostat works by correcting system temperature during the simulation with exponential decay.[30]

Thus, the optimal initial configuration of the system is obtained and used for the following MD simulations.

2.2.2.1 Annealing simulations

In order to study overall PG pyrolysis and assess the products formed, a temperature regime was employed to get the system at the desired final temperature. Then, the temperature was increased linearly for 500 ps to reach the desired maximum temperature (T_{Max}). This was done to give the system time to adjust to these temperature changes and to properly predict reaction pathways (temperature increase stage). The system remained at this temperature for another 500 ps (isothermal stage). Thus, a total of 10,100,000 iterations, or a simulation time of 1010 ps, were needed. A 10fs damping constant and a time step of 0.1fs/iteration were applied throughout these simulations. It is a common practice in ReaxFF to employ high temperatures (*e.g.* up to 4600 K) in order to get results in real-time.[31] Initially, simulation temperatures were set between 3000 K and 3750 K with an incremental temperature ΔT of 250 K. This was changed to 100 K when further simulations were conducted to generate more refined data. Three random simulations were conducted for each temperature.

2.2.2.2 Isothermal simulations

To study reaction kinetics, isothermal simulations were conducted to obtain reaction rate constants. The equilibrated system was subjected to temperatures from 2000 K to 4000 K at 250 K intervals for 10 ps (for every temperature) with a 100fs damping constant. Triplicates were also performed in this stage. As stated in literature and based on our simulations, such high temperatures do not affect kinetic rate constants since the relationship between ln(K) and 1/T is generally linear, and data at high temperatures can be interpolated to lower temperatures.

2.2.3 ReaxAMS computations

Small scale (at most 5 molecules) calculations were performed using ReaxAMS, which is an SCM product that combines SCM's ADF and BAND functionalities with reactive molecular dynamics in one interface.[26] The purpose of ReaxAMS was to study separately each elementary reaction involved in PG pyrolysis. Unlike ReaxFF-MD, the focus here was not on product concentrations and trends with respect to time. In fact, time is not a factor in these small-scale computations. The path the reaction takes, from reactant to product, was rather studied from an energy perspective. For every reaction, geometry optimizations for initial and final systems were computed, first using the universal force field (UFF) to improve bond lengths and angles, and then CHO.ff to minimize the energy on the specified molecule. The Nudged Elastic Band (NEB) method was then applied on the two systems to predict the energy path. This optimizes the intermediate 'images' to find the lowest energy possible from one image to the next. Spring forces along the band between images were added, the potential perpendicular to the band found and projected out, predicting the next image. From the energy path found, transition states and associated energies (Gibbs free energy, bond energies and enthalpies) were extracted.

3. Results and discussion

3.1 Experimental results

3.1.1 Product concentrations

Table 1 summarizes the results of PG pyrolysis under an inert atmosphere. Our results showed that thermal decomposition started at around 160 °C (433 K) and increased with temperature producing mainly PA and Ace.

3.1.2 Reaction mechanisms

The degradation of PG under an inert atmosphere is expected to proceed mainly via dehydration reactions as depicted in Fig. 3. PA and Ace, the direct products of dehydration of PG, were detected at relatively low temperatures, and they constituted the majority of the products formed (PA and Ace constituted 61% and 26% of the total weight of carbonyls detected). At higher temperatures, minimal amounts of FA and AA were detected, in addition to trace amounts of MGA and GA. To account for all these products reaction pathways were suggested and their corresponding kinetic parameters were estimated based on experimental results. In the first reaction step, PG loses one water molecule to give propylene oxide (PO) as an intermediate. The generation of propylene oxide via this pathway was validated by a computational study.[13] Also, a recent report discussed the presence of these species in e-cigarette aerosols.[32] Epoxide can undergo ring opening to give two other intermediates, namely propen-1-ol (P1) and/or propen-2-ol (P2) (Eqs 2 and 3).[33] These intermediates are just the enol forms of their corresponding carbonyls; propene-1-ol can tautomerize to give PA (Eq. 4), and propene-2-ol can tautomerize to give Ace (Eq. 5). On a less prominent route, the enols can undergo C=C bond cleavage to give smaller molecules including FA, AA, and ethylene (Eqs 6 and 7). Eq. 8 illustrates a transformation known as glycol cleavage in which a vicinal diol molecule undergoes C-C bond cleavage

Table 1. PG pyrolysis products (g/m^3) under N_2 at different temperatures and N_2 flow rates (mL/min).

T(°C)	Flow Rate	PA	Ace	AA	FA	GA	MGA
160	386	0	0	0.00012	0	0.0008	0
360	271	0.00003	0.00065	0.00009	0	0.00181	0
460	236	0.01248	0.00356	0.00192	0	0.00241	0
565	209	0.11391	0.03911	0.00575	0.00164	0.00321	0.00384
670	187	0.14963	0.07464	0.01648	0.00844	0.0045	0.00085

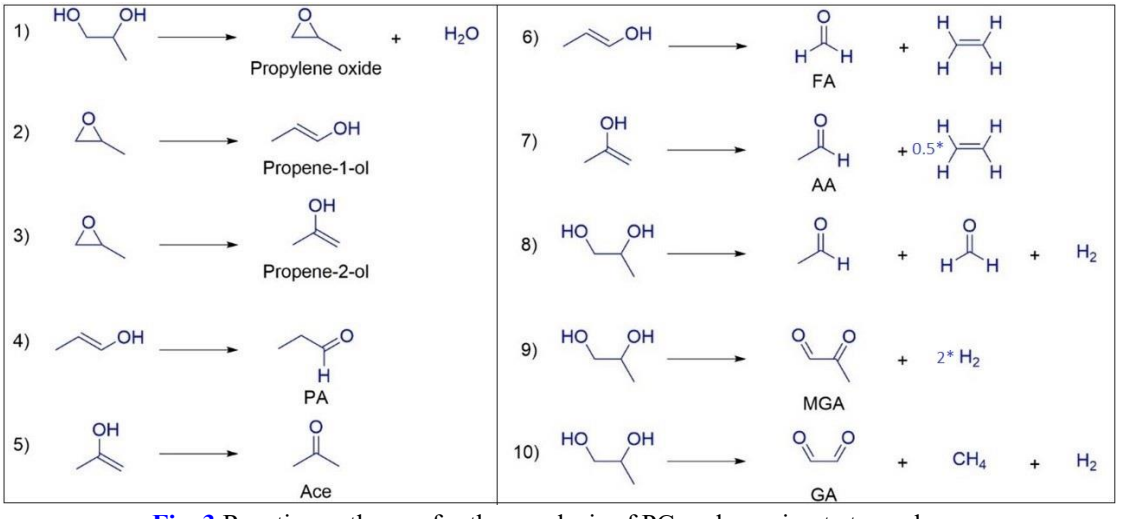

Fig. 3 Reaction pathways for the pyrolysis of PG under an inert atmosphere.

to give smaller carbonyls (FA and AA in this case).[34] This cleavage is usually catalyzed by a metal-based catalyst, which is not the case in our system, thus it is less noteworthy in our mechanistic study. Another minor transformation is the direct oxidation of the two alcohol functional groups to give MGA and a hydrogen molecule, via dehydrogenation reaction (Eq. 9).[8] Oxidation can be accompanied with C-C bond cleavage leading to the formation of GA (Eq. 10). MGA and GA were detected in trace amounts. It should be noted that the possible presence of small molecules like ethylene, methane and hydrogen gases was not verified in our experiment.

This scheme is in accordance to the one proposed by Laino *et al.*[3] for the decomposition of PG where PA and Ace form from the dehydration reaction. In fact, it adds more possible pathways such as FA and AA formation from dehydration and formation of GA and MGA from dehydrogenation reactions.

3.1.3 Kinetic model pathways

A proposed kinetic model incorporating reactions 1-10 is illustrated in Fig. 4. Products whose concentrations were not measured were ignored and assumed not to affect reaction rate constants.

The mole balance for PG is obtained by combining reaction 1 with 8, giving:

$$\frac{d[PG]}{dt} = (-k1 - k8)[PG] \tag{3}$$

Reactions 1 to 8 were assumed to follow the quasi-steady-state approximation. This has been done since the intermediates—namely *P*O, *P*1 and *P*2—were not detected, as will be later on shown, in the ReaxFF-MD simulations. In fact, experimentally, these intermediates were not detected either. However, these compounds do form, they are presented in other literature,[3] and *P*1 and *P*2 radicals appear in ReaxFF-MD simulations.

Adding reactions 2-5 and 7-8 yields the following expressions for *P*O, *P*1, and *P*2 concentrations:

$$[\text{Reaction 2} + \text{Reaction 3}]: \frac{d[PO]}{dt} = k1[PG] - (k2 + k3)[PO]$$

$$[PO] = \frac{k1[PG]}{[k2+k3]} \tag{4}$$

$$[\text{Reaction 4} + \text{Reaction 6}]: \frac{d[P1]}{dt} = k2[PO] - (k4 + k6)[P1]$$

$$[P1] = \frac{k1 \times k2[PG]}{[k2+k3] \times [k4+k6]} \tag{5}$$

$$[\text{Reaction 5} + \text{Reaction 7}]: \frac{d[P2]}{dt} = k3[PO] - (k5 + k7)[P2]$$

$$[P2] = \frac{k1 \times k3[PG]}{[k2+k3] \times [k5+k7]} \tag{6}$$

Substituting the expressions of *P*O, *P*1, and *P*2 in the mole balances of PA, Ace, FA, and AA yields the following modified mole balances:

$$\frac{d[PA]}{dt} = k4[P1] = \frac{k4(k1 \times k2)[PG]}{(k2+k3)(k4+k6)} \tag{7}$$

$$\frac{d[Ace]}{dt} = k5[P2] = \frac{k5(k1 \times k3)[PG]}{(k2+k3)(k5+k7)} \tag{8}$$

$$\frac{d[FA]}{dt} = k8[PG] + \frac{k6(k1 \times k2)[PG]}{(k2 + k3)(k4 + k6)} = \left(k8 + \frac{k6(k1 \times k2)}{(k2+k3)(k4+k6)}\right)[PG] \tag{9}$$

$$\frac{d[AA]}{dt} = k8[PG] + \frac{k7(k1 \times k3)[PG]}{(k2+k3)(k5+k7)} = \left(k8 + \frac{k7(k1 \times k3)}{(k2+k3)(k5+k7)}\right)[PG] \quad (10)$$

The reaction rates were defined as:

$$r_{PA} = \mathrm{K}_1[PG] \quad (11)$$

$$r_{Ace} = \mathrm{K}_2[PG] \quad (12)$$

$$r_{AA} = (\mathrm{K}_3+\mathrm{K}_5)[PG] \quad (13)$$

$$r_{FA} = (\mathrm{K}_4+\mathrm{K}_5)[PG] \quad (14)$$

$$r_{GA} = \mathrm{K}_6[PG] \quad (15)$$

$$r_{MGA} = \mathrm{K}_7[PG] \quad (16)$$

The number of reaction rate constants that will be estimated in the model was reduced from ten ($k1$ to $k10$) to seven (K1 to K7), with K1 to K7 defined by,

$$\mathrm{K1} = \frac{k4(k1 \times k2)}{(k2+k3)(k4+k6)} \quad (17)$$

$$\mathrm{K2} = \frac{k5(k1 \times k3)}{(k2+k3)(k5+k7)} \quad (18)$$

$$\mathrm{K3} = \frac{k6(k1 \times k3)}{(k2+k3)(k5+k7)}; \quad (19)$$

$$\mathrm{K4} = \frac{k7(k1 \times k2)}{(k2+k3)(k4+k6)}; \quad (20)$$

and,

$$\mathrm{K5} = k8 \quad (21)$$

$$\mathrm{K6} = k10 \text{ (for GA)} \quad (22)$$

$$\mathrm{K7} = k9 \text{ (for MGA)} \quad (23)$$

All reaction rate constants, K (s^{-1}), were assumed to follow the Arrhenius equation,

$$\mathrm{K} = A_0 \times e^{-Ea/R \times T} \quad (24)$$

With A_0: pre-exponential term (1/s), T: temperature (K), Ea: Activation energy in (J/mole), R: ideal gas constant (J/mol.K). The parameter estimation toolbox in Matlab was used to estimate the Arrhenius constants that minimize the square of the errors between experimental results and model predictions.

3.1.4 Model validation

The estimated activation energies for the rate constants of equations (17) – (23) are summarized in Table 2.

PG degradation under N_2 atmosphere mainly produced propanal starting at 360 °C which continued to increase dramatically as the temperature reached 565 °C. Similarly, Acetone was produced but to a lesser extent. This 1 can be explained by PG degradation favoring the formation of propylene-oxide intermediate at low temperatures, under which it degrades to propene-1-ol and propene-2-ol along paths 1-2-4 and 1-3-5 as shown in Fig. 4.

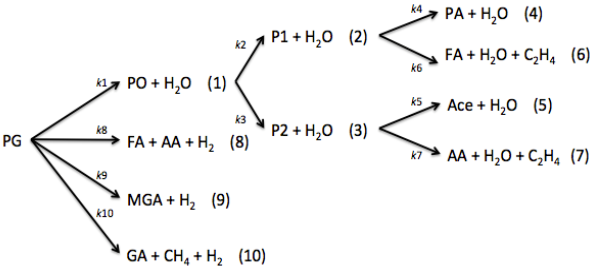

Fig. 4 Proposed kinetic model for PG thermal degradation.

As the temperature is increased, PG and propene-ols underwent further cracking to produce new carbonyls including FA and MGA from side reaction pathways 1-2-6 and 1-3-7 along with side reactions 8, 9 and 10. PA product formation slowed down as a result of the new side-products being formed above 565 °C as shown in Fig. 5 and Fig. 6. This kinetic behavior was captured by the degradation model which showed an excellent agreement with the experimental results of all products.

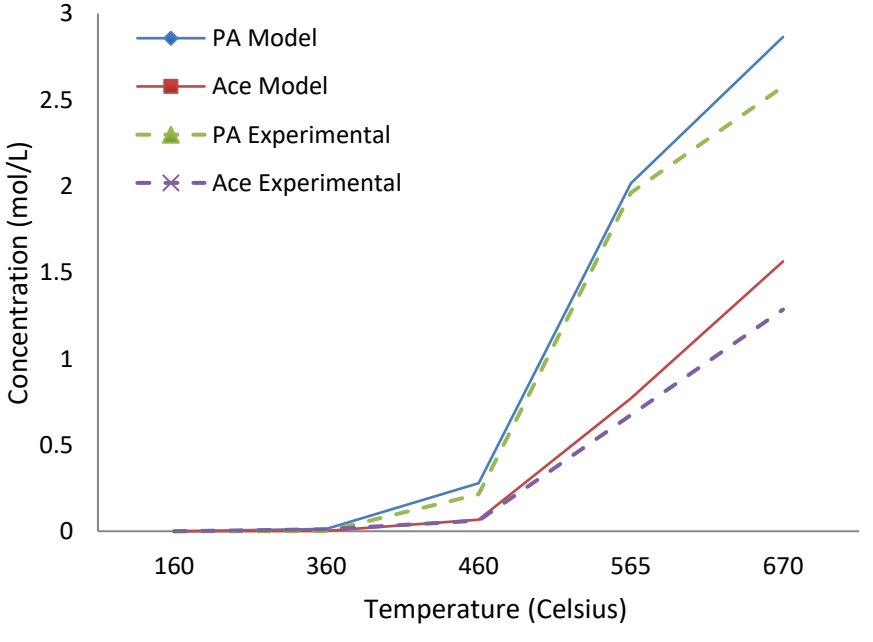

Fig. 5 Experimental versus predicted concentration at different temperatures for PA and Ace.

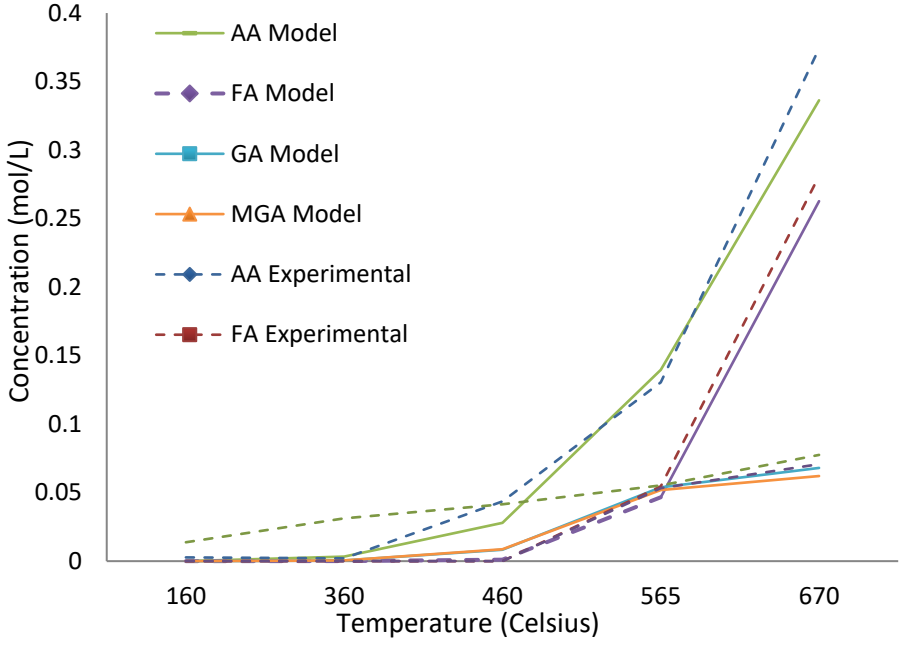

Fig. 6 Experimental versus predicted concentration of products at different temperatures for AA, FA, GA, and MGA.

Table 2. Estimated activation energies (J/mol).

Activation energy from rate constant	K1	K2	K3	K4	K5	K6	K7
Ea (J/mol)	1.14×10^5	1.4×10^5	2.41×10^5	1.86×10^5	1.64×10^5	1.17×10^5	1.14×10^5

3.2 ReaxFF-MD results

3.2.1 Product distribution

The simulation results from both annealing and isothermal simulations were assessed first with the Reaction Event Detection tool in ReaxFF's ChemTraYzer. This tool helps in viewing the radicals formed throughout the simulation time, the time of formation of these radicals (via a timeline), the elementary reactions involved, and the rates and fluxes of these reactions. One can also observe all the pathways involved with a certain molecule, where it is involved as a reactant, or as a product. PG undergoes pyrolysis as shown in Fig. 7.

The supplementary data (Fig. S1 through Fig. S4) further elaborates the mechanisms obtained from ChemTraYzer.

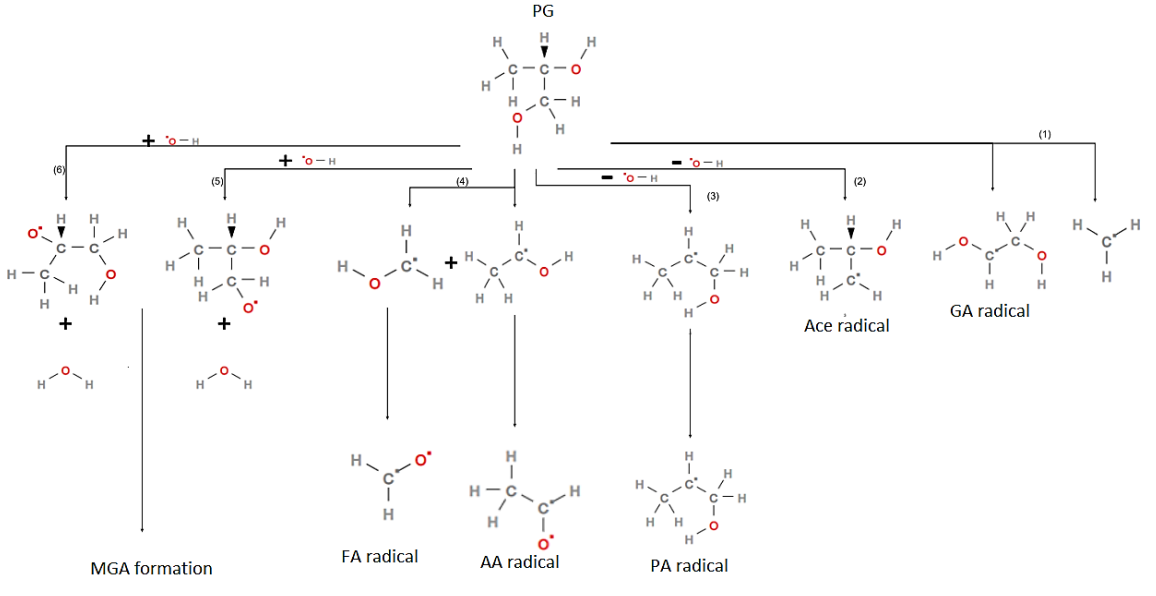

Fig. 7 Main reaction pathways of PG pyrolysis from ChemTraYzer analysis from ReaxFF-MD simulations. Captions (1) to (7) indicate each possible pathway.

From the timeline and the reactions taking place in ChemTraYzer, a simple mechanism was employed where PG decomposes to give each of the following products:

- CH_2O or FA
- C_2H_4O or AA
- C_3H_7O or PA/Ace radical
- $C_2H_4O_2/C_2H_5O_2$ or GA radicals
- $C_3H_5O_2/C_3H_4O_2$ or MGA radical

These products are in accordance to the ones obtained in the previous section and other literature.[3] It is important to note that the formation of radicals for a certain molecule varied with temperature; noting each at every run was done to ensure the molecule in question is properly recorded. After examining the reaction events in every run, every molecule's (or radical's) number (N) versus iteration. xy file was extracted. All simulations were repeated three times to ensure accuracy and reliability of the results. Fig. 8 shows the averaged N versus time of all the species at T_{Max} of 3250 K.

The number of molecules initially remains at 10 indicating PG has not yet started decomposition. Species start forming from PG pyrolysis at around 2500K with a sharp increase in molecules at 3000K. Decomposition thus occurs prior to reaching the isothermal temperature.

Figures 9a, b and c show the evolution of the different PG pyrolysis products for the case of T_{Max} = 3250 K. Simulations have shown that PG started completely decomposing at simulation temperatures above 3000 K. It fully decomposes to produce numerous carbonyls, as shown in Fig. 9. FA did not form as soon as PG decomposed, but soon after, it gradually increased to reach maximum values. Similarly, AA formed later during the simulation, increasing somewhat linearly, then decomposing to reach almost zero value. It possibly formed smaller carbonyl chains such as CH_2O, CH_3, and lighter gases such as H_2 and H_2O. The PA/Ace radical was formed in spikes, nonetheless, it appeared first relatively to other aldehydes, suggesting that it might be forming directly from PG degradation. In fact, isothermal simulations further showed that these two molecules, especially PA, formed as soon as PG started degrading.

GA formed early on in the simulation, around the time PG started decomposing, which was expected, as GA is a longer chain carbonyl with more oxygen atoms than FA and AA. It reached a low maximum N value and decreased back to zero, as it decomposed further into smaller carbon chains. MGA formed in spikes and did not reach high N values. This was expected since MGA is a relatively long chain hydrocarbon that will decompose to give smaller carbonyls and shorter molecules.

In addition, H_2O is a direct product of PG dehydration and formed as soon as PG decomposed. It kept increasing as it was formed from other carbonyls. H_2 appeared later in the simulation and increased as it was formed from carbonyl dehydrogenation. It then decreased which could be attributed to the formation of carbonyls possessing single bonds. The abundance of H_2O over H_2 indicates that dehydration is favored over dehydrogenation.

3.2.2 ReaxFF-MD kinetics

The rates of formation of the carbonyls were calculated from ReaxFF-MD isothermal simulations over the temperature range of 2000 K-4000 K. In general, it was found for a carbonyl *A* as follows,

$$Rate\ formation_A = \frac{(N_{A\_formed} - N_{A0})}{time\ of\ formation_A} \quad (25)$$

Where N_{A_formed} is the number of *A* molecules formed at the time of formation and N_{A0} is the initial number of A molecules.

From equations (11) to (16), the rate constants were obtained at each simulation temperature. The Arrhenius equation $K = A_0 \times e^{-Ea/R\times T}$ (24) was then employed in logarithmic form to find the Arrhenius parameters of each carbonyl:

$$\ln(K) = -\frac{Ea}{R\times T} + \ln(A0) \quad (26)$$

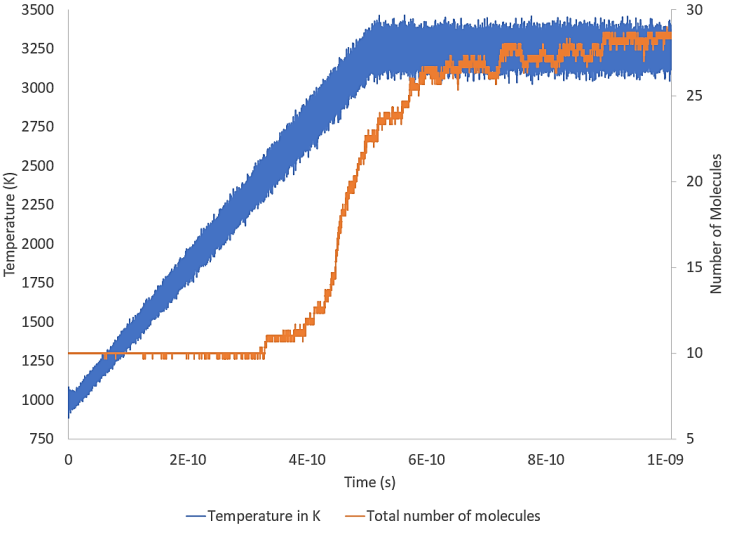

Fig. 8 Averaged total number of molecules over time, along with the temperature profile, at TMax = 3250K.

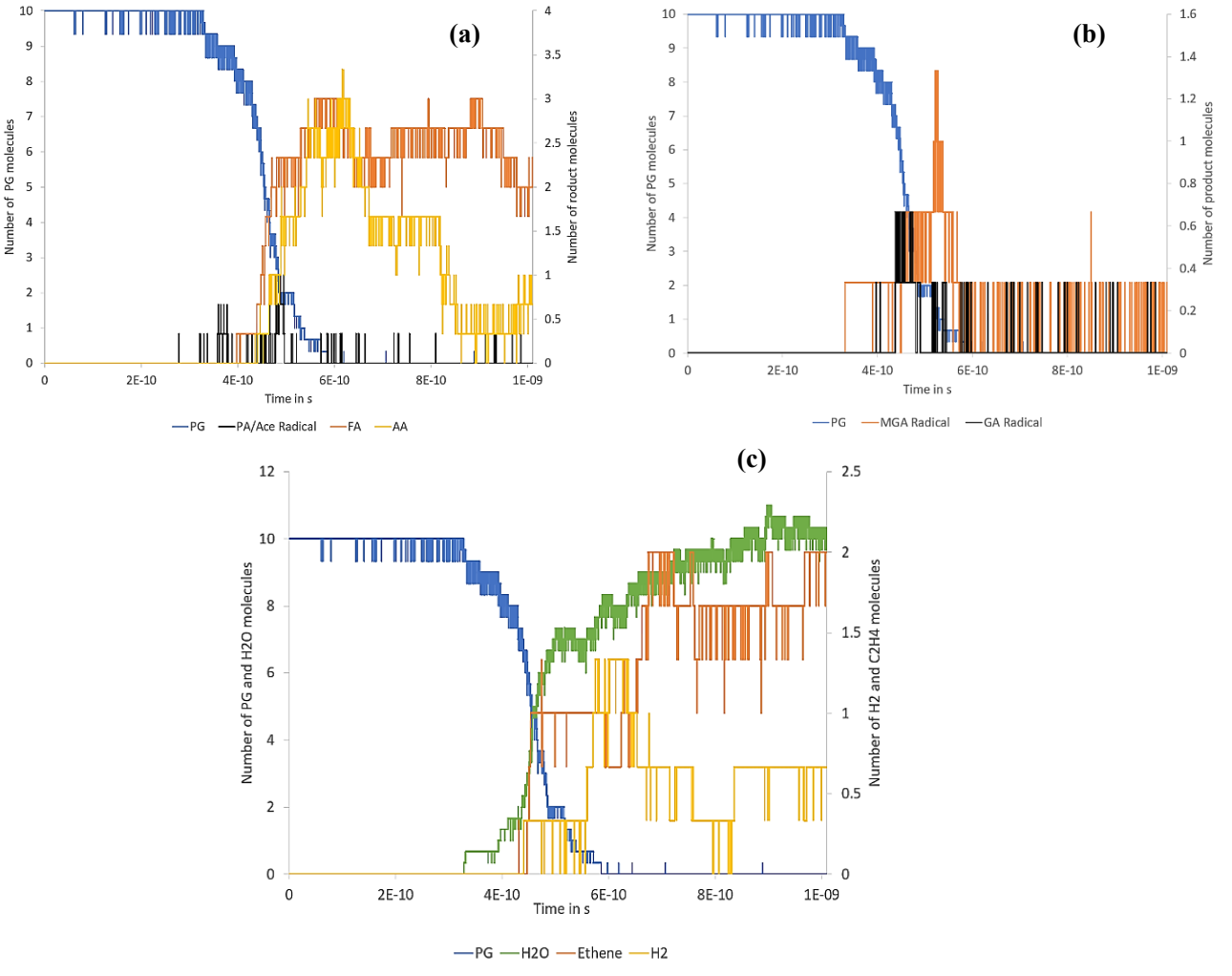

Fig. 9 Number of molecules distribution over time for T_{Max} = 3250K. (a) time evolution of molecules for PG, AA, FA and PA (b) time evolution of molecules for PG, MGA and GA (c) time evolution of molecules for PG, H_2O, H_2 and C_2H_4.

Plotting ln(K) versus $\frac{1}{T}$ should give a line with slope $-\frac{Ea}{R}$ and an intercept of ln(A_0) as seen in Fig. S5 to Fig. S10. The calculated Ea and A_0 for the proposed pyrolysis mechanism reactions are summarized in Table 3. For the experimental model, rate constants K1 to K7 were found, however, in order to clarify each formation reaction, the K-values are as follows based on equations (11) through (16)

- *K1*: k value for PA formation
- *K2*: k value for Ace formation
- *K3* + *K5* was summed up to give k value for AA formation
- *K4* + *K5* was summed up to give k value for FA formation
- *K6*: k value for GA formation
- *K7*: k value for MGA formation

For the dehydration-related products, Ace formation has the lowest activation energy barrier from ReaxFF-MD, however, it does not appear in abundance or across the whole temperature range as further provided in the supplementary data (Fig. S6). Thus, between PA, AA and FA, the reaction constant for PA formation exhibited the lowest activation energy, meaning it is the most favored reaction. This is in accordance with experimental results where PA was the most detected aldehyde, with the highest concentrations, and formed at low temperatures. It was formed most readily in ReaxF-MD although at lesser concentrations when compared

Table 3. Activation energy values (J/mol) of carbonyl formation from ReaxFF-MD and compared to experimental results.

	Activation energy from rate constant k-formation of:					
	PA	Ace	AA	FA	GA	MGA
Experimental model Ea (J/mol)	1.14E+05	1.40E+05	1.64E+05	1.64E+05	1.17E+05	1.14E+05
ReaxFF-MD Ea (J/mol)	1.11E+05	8.52E+04	1.41E+05	1.73E+05	1.06E+05	1.33E+05
Error with respect to experimental model	3%	39%	14%	5%	9%	17%

Table 4. Pre-exponential factor (1/s) values of carbonyl formation from ReaxFF-MD.

	Pre-exponential factor from rate constant k-formation of:					
	PA	Ace	AA	FA	GA	MGA
A_0 (1/s)	1.63E+12	3.99E+12	4.95E+12	1.41E+13	2.98E+12	5.65E+12

to FA. This could be attributed to the fact that FA is formed from other side decomposition reactions of longer chain carbonyls (AA, PA, Ace, GA and MGA). In addition, previous literature employing DFT calculations[3] has shown that the formation of PA from PG dehydration is favored over that of Ace.

As for dehydrogenation mechanism, both rate constants for GA and MGA formation exhibit close values, however, in both ReaxFF-MD and experiments, GA was detected across the temperature range while MGA was not a favored product.

The high values of A_0 obtained indicate a high frequency of molecule collisions as presented in Table 4. Pre-exponential factor (1/s) values of carbonyl formation from ReaxFF-MD.. In fact, FA formation rate constant exhibits the largest value and indicates the abundance of FA formed.

3.2.3 PG overall thermal degradation

Another approach to assessing PG pyrolysis is studying the overall decomposition of PG. Therefore, the rate of PG decomposition $k_{PG\ decomposition}$ was found from ReaxFF-MD results. The total concentration profile of PG was extracted from every isothermal simulation (including triplicates per one T_{Max}) and the results were averaged for every T. Then the integrated first-order rate law was applied to determine $k_{PG\ decomposition}$ at each T:

$$\ln(N_t) = -k_{PGdecomposition} * t + \ln(N_0) \quad (27)$$

Where N is the number of PG molecules decomposing as the simulation progresses. Plotting ln (N_t) versus time t (in s) provides a linearly-fitted plot with a slope of $k_{PG\ decomposition}$. After finding the kinetic rate constants for the whole temperature range, they were linearly fitted using ln($k_{PG\ decomposition}$) versus 1/T in Fig. S11. Arrhenius parameters were then extracted from the linear fitting and presented in Table 5.

Table 5. Activation energy values (J/mol) and pre-exponential factor (1/s) values of PG decomposition from ReaxFF-MD.

	PG Decomposition
Ea	1.86E+05
A_0	6.84E+13

The results show that the A_0 values for PG decomposition are at least one order of magnitude larger than all k-formation terms, except for PA formation where PG decomposition is the same order of magnitude. In addition, the energy barrier to break PG bonds is higher than the ones for product formation. As will be later seen in ReaxAMS small-scale computations, for the PG molecule to crack, energy is needed to be inputted to the system (endergonic reaction), thus explaining the presence of a high energy barrier.

3.3 ReaxFF sensitivity analysis

3.3.1 Effect of temperature

Temperature played an important role during ReaxFF simulations and PG starts generating decomposition carbonyls at 2000 K, with increasing carbonyl concentrations at 2750 K. PA, GA and MGA radicals form over the whole temperature range of 2000 to 4000 K. FA and AA begin forming from 2500 up to 4000K. Finally, Ace, which is generally not detected in abundance in both experiments and MD, forms only between the 2000 to 3000 K range. Such high temperatures were chosen as it is a simulation condition where reactions in ReaxFF-MD are generally expected to occur, as seen in literature.[31]

3.2.2 Effect of density

Density is an important input variable that needs to be optimized before precise simulations are run. By varying the volume of the box to 50^3 Å^3, 23^3 Å^3, and 18^3 Å^3, densities of 0.01, 0.1 and 0.22 g/cm^3 were obtained respectively. Simulations were run for T_{Max} values of 3000 K to 4000 K with 250 K intervals. N profiles were parsed, with the number of PG molecules detected compared at T_{Max} = 3250 K in Fig. 10 Number of PG molecules distribution for the three densities over time for TMax = 3250 K.

It can be seen that a density of 0.01 g/cm^3 does not lead to PG decomposing (except for a few points in time which can be considered as noise). This is attributed to the low collision of molecules. On the other hand, a density of 0.22 g/cm^3 shows a sharp decrease in PG molecules, with the reappearance of numerous spikes after its supposed decomposition. Here, side reactions are occurring, due to the high density and thus high collisions between all molecules involved. Nonetheless, the physical system, in the experiments specifically and the e-cigarette generally, do not produce propylene glycol gas during pyrolysis. At the 0.1 g/cm^3 density, PG decomposes less sharply than at 0.22 g/cm^3, nevertheless, it decomposes fully and does not reappear after its consumption.

In addition, pyrolysis products form in both densities 0.1 and 0.22 g/cm^3 T_{Max} = 3250 K, and in all densities as temperature increases. Therefore, to further study the difference between densities, k-formation values and Arrhenius fitting parameters were obtained. This has been done prior to the triplicates method as this was the preliminary test. The results are provided in the supplementary data in Table S1. All in all, increasing system density will increase particle collisions, initiate decomposition sooner, and speed up the decomposition of reactants, as noted in literature, such as the pyrolysis of n-dodecane.[27] As density was increased, activation energy and pre-exponential factors of

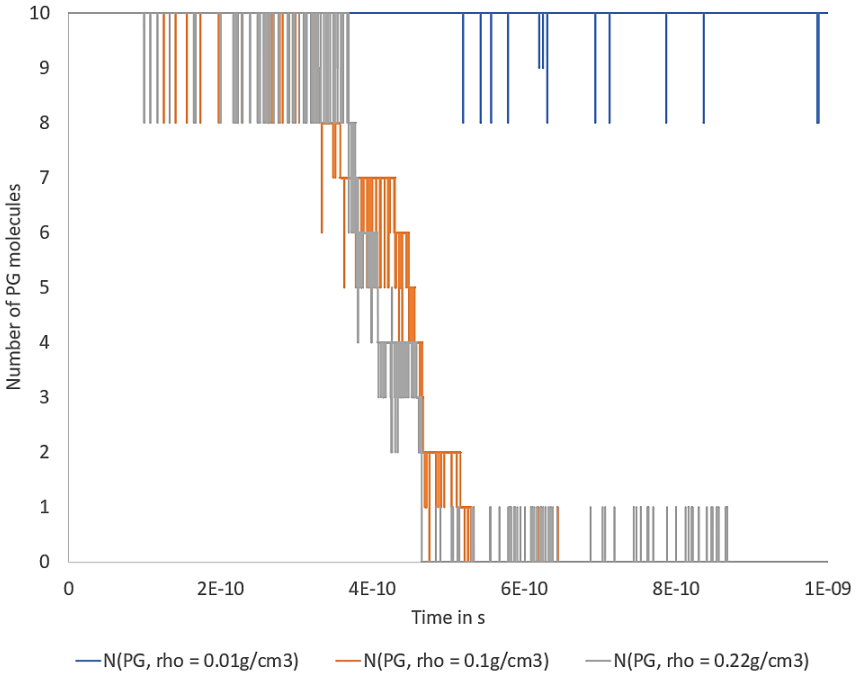

Fig. 10 Number of PG molecules distribution for the three densities over time for T_{Max} = 3250 K.

decomposition increased too, with the latter increasing at a faster rate. Temperature-depended simulations where then based on the system density (ρ=0.08g/cm^3) of which results showed closer Arrhenius values to those of experiments. Nonetheless, it has been concluded that the effect of temperature on the system and on the results is higher than the effect of density.

3.4 ReaxAMS results

3.4.1 Transition states and bond energies

The elementary reactions presented in Fig. 3 were simulated each on ReaxAMS using the NEB method. The energy pathways were computed, and transition states identified as illustrated in Fig. 11.

ReaxAMS calculated the bond energy of every system involved. The change in bond energy from reactants to products was determined, in addition to the change between transition states and reactants, and transition states and products. The values can be found in the supplementary data (Table S2).

Reaction information can be derived from bond energies and interpreted using the TS diagrams in Fig. 11. For instance, for reaction 1, energy was required to be added into the system to break the PG bonds. PG undergoes a C-O bond cleavage, and one O-H bond formation, with the oxygen still attached to the carbon in the molecule, to reach the TS. Then, the product resulted from the TS by an O-H cleavage (to obtain H_2O), and a C-O bond formation.

In reaction 2, taking the reactant to the TS involved a change in bond angles and lengths, with no bond cleavage. However, the TS underwent a C-O bond cleavage in the middle (C2), a hydrogen abstraction on the outer carbon atom (C1), resulting in the formation of an O-H bond and a double C=C bond between C1 and C2, resulting to a higher energy on the TS-product side.

For reaction 3, the outer carbon atom (not bonded with oxygen, *i.e.* C3) broke from C2. In addition, oxygen broke from C1, and bonds with a hydrogen atom abstracted from C2. A double bond formed between C1 and C2, and a single bond between C2 and C3.

In each of reactions 4 and 5, one O-H bond broke, and so did one bond of the C=C double bonds. One C-H bond was formed, in addition to a double C=O bond.

In reaction 6, one double C=C bond and one O-H bond broke. One C=O bond and one C-H bond formed FA. Finally, one C=C double bond and one C-H bond formed ethene.

In reaction 7, Propene-2-ol formed Ace as in reaction 5, then, each Ace molecule broke at the C-C bond between C1 and C2. Each of the two AA contained one C=O and one C-H bond on C2 and three C-H bonds on C3. Ethene formed from two CH_2 radicals bonding via a C=C bond.

For reaction 8, C-C bond cleavage between C1 and C2 resulted in the TS that then undergoes two O-H abstractions and a H-H bond formation–one H_2 molecule.

Reaction 9 involved −OH cleavage from C2, only to lose one hydrogen atom, and bonding again to C2 with a double bond. The other Oxygen atom also formed a double bond with C1 by losing a hydrogen atom. The resulting two hydrogen atoms bonded to form H_2. C1 and C2 both lose one hydrogen atom, and thus, another H_2 molecule is formed. MGA and two H_2 molecules resulted from reaction 9.

Reaction 10 contained two steps. In 10 (1), C3 broke off from C2 forming a $-CH_3$ radical. In step 10 (2), each oxygen lost one attached hydrogen and formed a double bond with carbon (two C=O bonds form). This was possible since carbon lost one attached hydrogen (three C-H bonds breaking). One

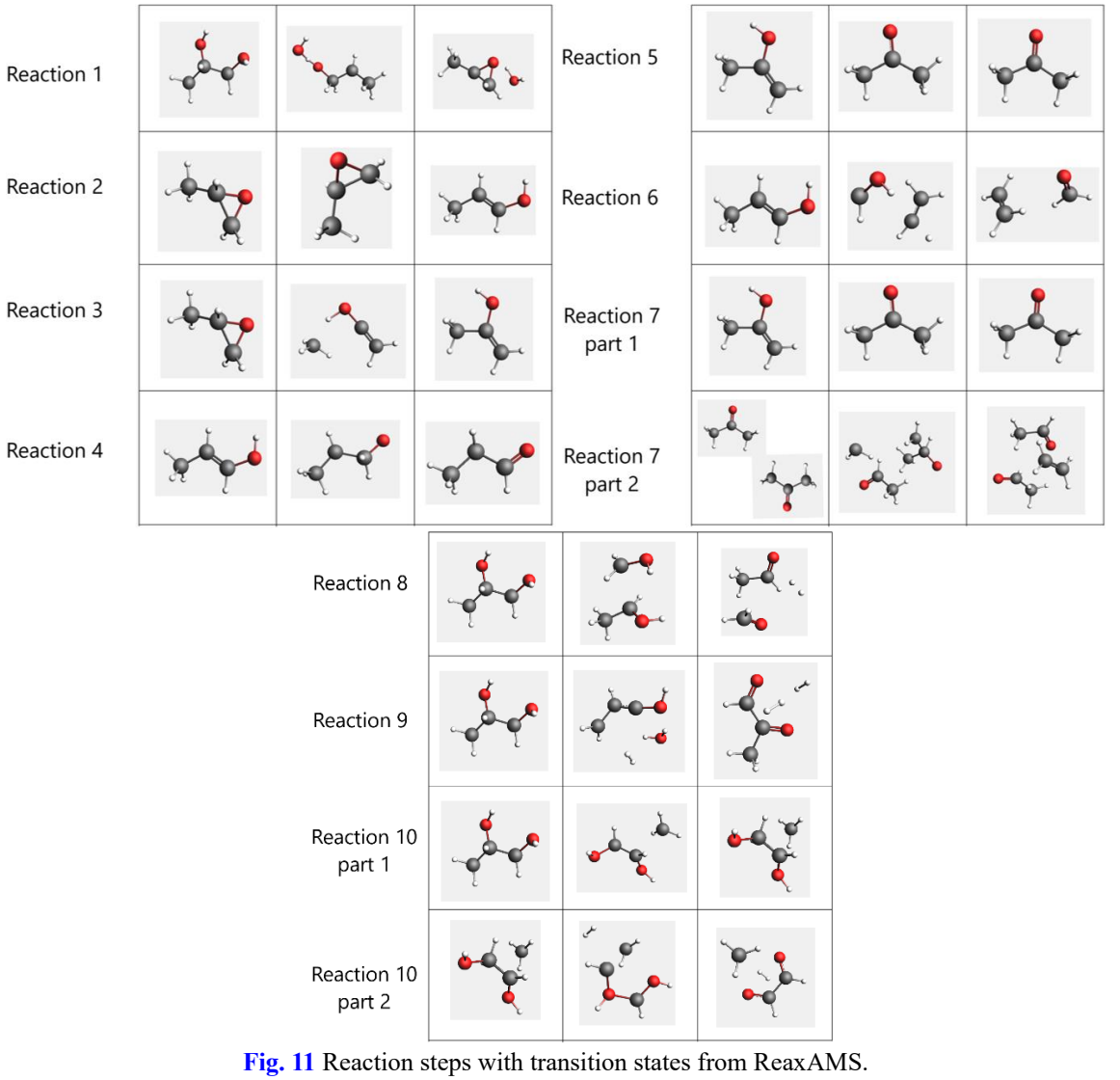

Fig. 11 Reaction steps with transition states from ReaxAMS.

C-H bond formed transforming CH_3 into CH_4. Finally, the two hydrogen atoms left formed one H-H bond, or H_2.

3.4.2 Enthalpy and Gibbs free energy

The enthalpy plots for reactions (1), (2) and (3) are shown in Fig. 12, while information for the other reactions can be found in the supplementary data. The temperature presented is 1000 K, which is close to the experimental condition where the temperature was highest and all products appeared, as seen in Table 1. It can be noted from the enthalpy changes between reactants and products, that only reactions 2 and 3 (and the second step of reaction 10) were exothermic, while the other reactions were endothermic.

It can be seen from the free energy profiles in Fig. 13 that reactions 2, 3, 6, and 7(2) are exergonic reactions, as they released free energy ($G_{final} < G_{initial}$), and thus occurred without the need of energy being added to the system (spontaneous reactions). The other reactions are endergonic, notably reaction 1, and therefore it need energy to proceed. Such energy initially originated from thermal heating and could also be attributed to the high-energy products formed in previous endergonic reactions.

4. ReaxAMS kinetics

To study favored pathways, small-scale computations were run on the individual reactions presented in Fig. 3 Reaction pathways for the pyrolysis of PG under an inert atmosphere.. For each reaction, the Gibbs free energy of the reactant and of the transition state were found. The change in these Gibbs free energies ($\Delta G^{\ddagger}$) was used to find the activation of each elementary reaction. Energy calculations were found over a temperature range similar to experimental temperatures (400K to 1000K at 100K increments). For each reaction, in order to obtain an accurate Ea value that applies over this temperature range, and rather than simply averaging $\Delta G^{\ddagger}$ obtained at each T, the following equation is applied:

$$k(T) = \frac{k_B T}{h} * \exp\left(\frac{\Delta G^{\ddagger}}{RT}\right) \quad (28)$$

Where k_B is the Boltzmann constant and h is the Plank constant. The logarithmic form of the Arrhenius equation was plotted for each k value, and the Arrhenius parameters are found. The activation energies of the elementary reactions are presented

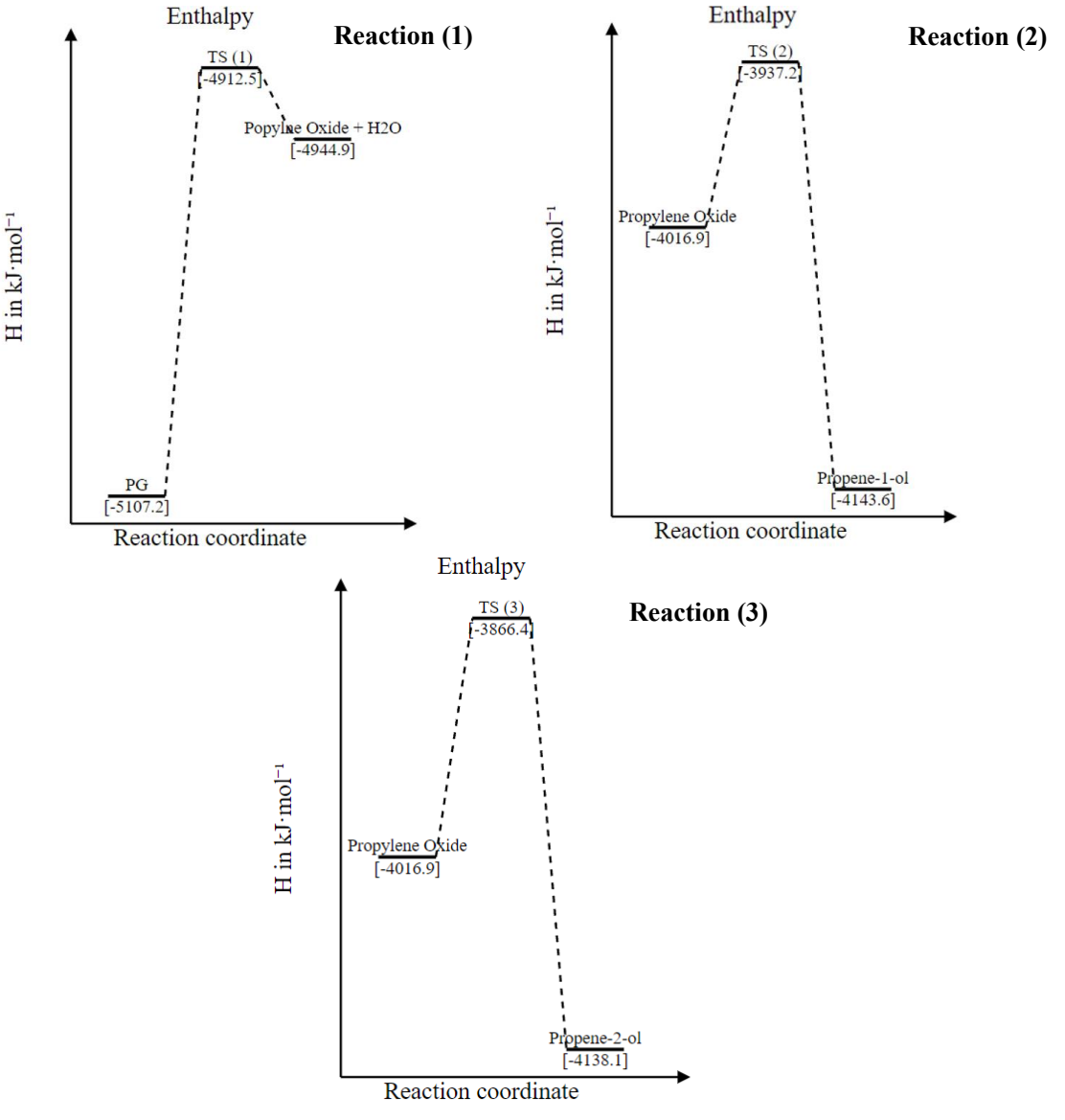

Fig. 12 Reactions (1), (2) and (3) enthalpies with respect to reaction coordinate at 1000K.

Table 6. Ea values (J/mol) of pathway reactions of PG Pyrolysis from ReaxAMS.

Mechanism	1	2	3	4	5	
Ea (J/mol)	2.04E+05	8.71E+04	1.58E+05	2.82E+05	3.64E+05	
Mechanism	6	7 (2)	8	9	10 (1)	10 (2)
Ea (J/mol)	7.50E+05	6.00E+05	2.91E+05	1.07E+06	3.23E+05	7.80E+05

in Table 6. Note that this section covers the activation energy of the reaction steps and not the overall formation of certain products. The aim of this section is to cover the preferred pathways rather than focus on rate of overall aldehyde formation.

As shown in Fig. 14, PG can undergo cracking from either pathways (1), (8), (9), or (10). From the activation energy barriers, pathway (1)—the dehydration of PG—has the lowest Ea value and is thus the preferred reaction. It shows similar barrier heights to the one computed by Laino *et al.* for the same reaction ($\Delta G^{\ddagger}$=66.5kcal/mol or 2.78E+05 J/mol)[3] which was also considered the preferred pathway. This further justifies why more dehydration products (PA, Ace, FA, and AA) were detected over dehydrogenation products (GA and MGA) in experiments and ReaxFF-MD. Pathway (2), prop-1-ol formation from PO, had the lowest activation energy and was thus the favored reaction in PG pyrolysis. The next lowest was pathway (3), the formation of prop-2-ol from PO. After prop-1-ol formation, two pathways can occur: the formation of PA—pathway (4)—and the formation of FA—pathway (6).

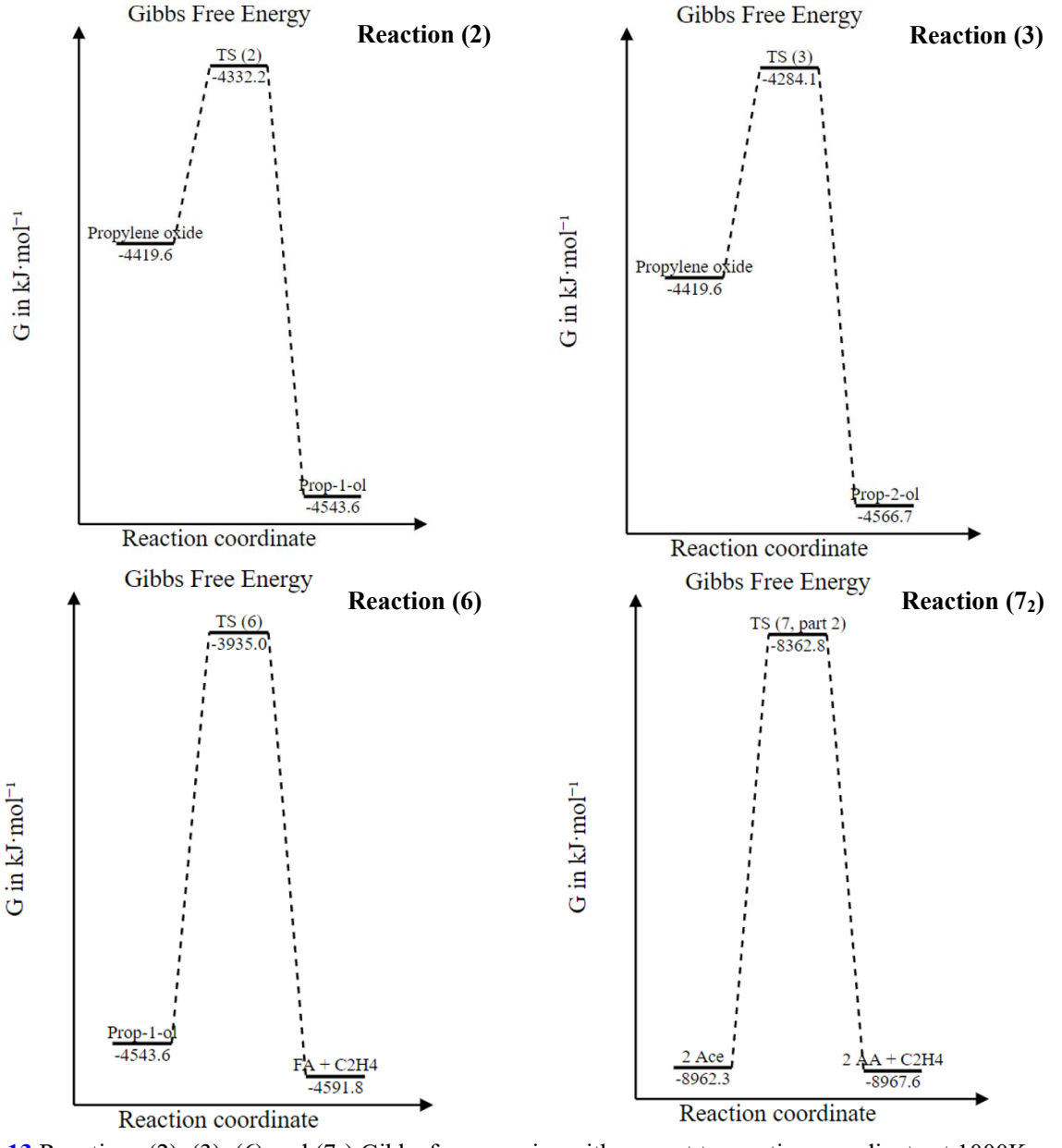

Fig. 13 Reactions (2), (3), (6) and (7_2) Gibbs free energies with respect to reaction coordinate at 1000K.

From elementary reaction activation energies, one can deduce that pathway (4) is the preferred reaction from prop-1-ol, thus, PA formation is the dominant pathway. While Laino *et al.* model PA forming directly from PO, our work proposes the intermediate step of prop-1-ol formation. Nonetheless, similar barrier heights are observed for this PA formation step: 2.45E+05 J/mol at 800K[3] 2.82E+05 J/mol (our work).

The same reasoning is applied for reactions of prop-2-ol (pathways 5 and 7), where pathway (5)—formation of Ace—is the preferred pathway over AA formation. Comparing Ace formation barrier height from literature, Lano *et al.* DFT methods computed 2.80E+05 J/mol at 800 K[3] and our work computed 3.64E+05 J/mol, over the temperature range.

5. Conclusion

In this study, experimental data was used to develop a kinetic model to estimate the activation energies of PG degradation over a temperature range of 160-670 °C (333-943 K), and under an inert N_2 atmosphere where the dominant degradation pathway was found to be the dehydration of PG to give PA and Ace. We employed high-temperature MD simulations to investigate further these findings and the main products observed were propanal, acetone, formaldehyde, acetaldehyde, glyoxal and methyl glyoxal. FA was a dominant product that could form from several cracking reactions. PA formation reaction had the lowest activation energy and proved to be the dominant pathway.

Elementary reactions were studied in ReaxAMS to determine energies and transition states. Rate-limiting steps and favored pathways were identified in addition to bond formation and breakage mechanisms. PG pyrolysis favored the pathway of propylene oxide to prop-1-ol and prop-2-ol. These are exergonic and exothermic, and their products lead to the direct formation of PA and Ace, corroborating

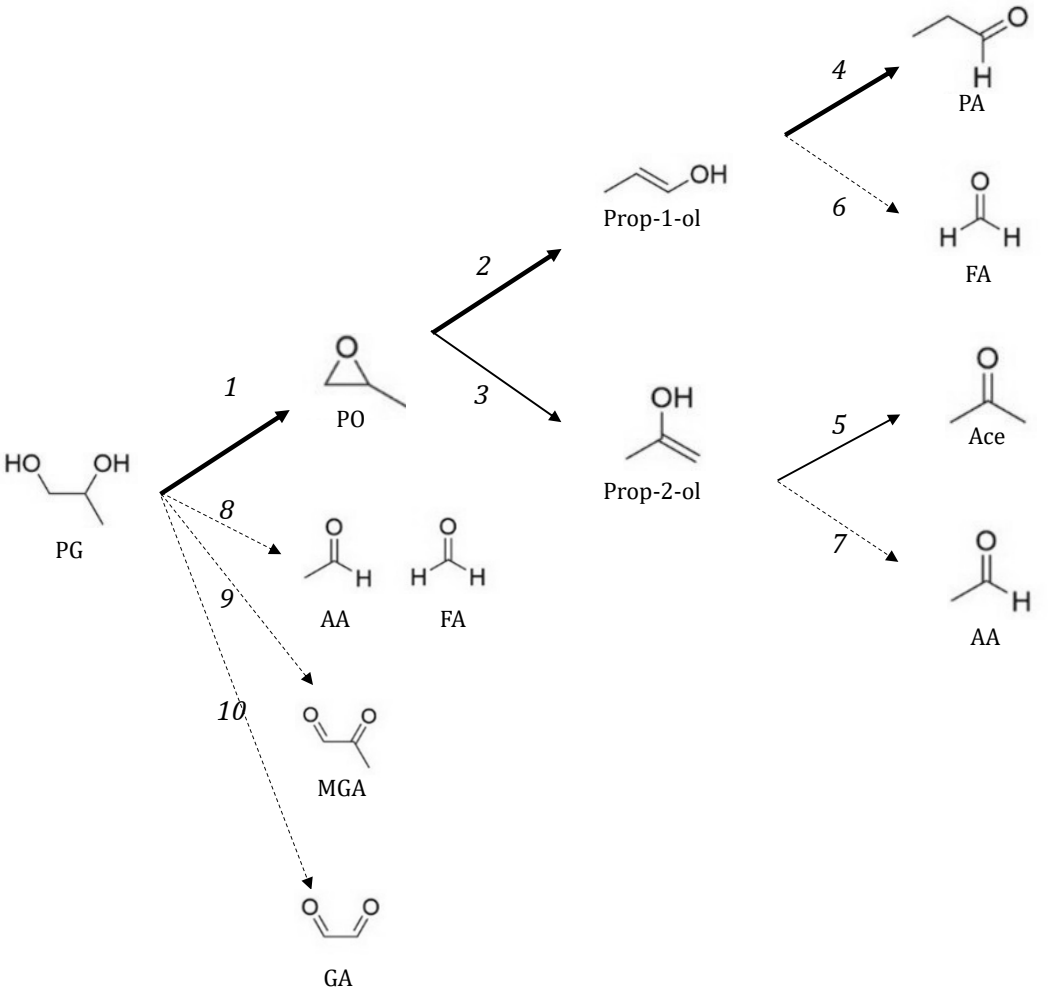

Fig. 14 Dominant and least preferred pathways for PG pyrolysis.

experimental and MD findings. Similar to ReaxFF-MD and experimental results, the formation of PA and Ace respectively were the dominant pathways. In addition, the formations of FA and AA respectively, were found to be exergonic while all elementary reactions that have PG as reactant were endothermic and endergonic.

Future work will concentrate on the oxidative degradation of PG to account for the formation of oxygenated carbonyls observed in ECIG emissions. Other e-liquids and flavors could be studied using the same methodology.

Acronyms

A_0 pre-exponential factor
Ea activation energy
T_{Max} maximum temperature
AA acetaldehyde
Ace acetone
DFT Density Functional Theory
EFF empirical force fields
FA formaldehyde
GA glyoxal
GUI Graphical User Interface
MD molecular dynamics
MGA methylglyoxal
NEB The Nudged Elastic Band
NVT Number-Volume-Temperature
P1 propen-1-ol
P2 propen-2-ol
PA propanal
PG Propylene Glycol
PO Propylene Oxide
QM quantum mechanics
R ideal gas constant
ReaxAMS Amsterdam Modeling Suite
ReaxFF-MD Molecular Dynamics Reactive Force Field
SCM Software for Chemistry and Materials
TS transition state
UFF universal force field

Acknowledgments

This work was supported by the National Institute on Drug Abuse of the National Institutes of Health (NIH grant number P50DA036105) and the Center for Tobacco Products of the U.S. Food and Drug Administration (FDA). The content is solely the responsibility of the authors and does not necessarily represent the official views of NIH or FDA.

Conflict of Interest
The authors declare no conflict of interest.

Supporting information
Applicable

References

[1] M. A. McGowan, A. Scheman, S. E. Jacob, Propylene glycol in contact dermatitis: a systematic review, *Dermatitis*, 2018, **29**, 6-12, doi: 10.1097/DER.0000000000000307.

[2] W. J. RossiterJr, M. Godette, P. W. Brown, K. G. Galuk, An investigation of the degradation of aqueous ethylene glycol and propylene glycol solutions using ion chromatography, *Solar Energy Materials*, 1985, **11**, 455-467, doi: 10.1016/0165-1633(85)90016-4.

[3] T. Laino, C. Tuma, P. Moor, E. Martin, S. Stolz, A. Curioni, Mechanisms of propylene glycol and triacetin pyrolysis, *The Journal of Physical Chemistry A*, 2012, **116**, 4602-4609, doi: 10.1021/jp300997d.

[4] Y. Zhao, L. Ding, J. Liu, H. Yang, X. Yin, S. Tuo, Q. Zhang, Pyrolysis characteristics of different humectant at high temperature, *Asian Journal of Chemistry*, 2014, **26**, 4893-4896, doi: 10.14233/ajchem.2014.16580.

[5] S. Han, H. Chen, X. Zhang, T. Liu, Y. Fu, Levels of selected groups of compounds in refill solutions for electronic cigarettes, *Nicotine & Tobacco Research*, 2016, **18**, 708-714, doi: 10.1093/ntr/ntv189.

[6] A. Breland, E. Soule, A. Lopez, C. Ramôa, A. El-Hellani, T. Eissenberg, Electronic cigarettes: what are they and what do they do? , *Annals of the New York Academy of Sciences*, 2017, **1394**, 5-30, doi: 10.1111/nyas.12977.

[7] A. EL-Hellani, R. Salman, R. El-Hage, S. Talih, N. Malek, R. Baalbaki, N. Karaoghlanian, R. Nakkash, A. Shihadeh, N. A. Saliba, Nicotine and carbonyl emissions from popular electronic cigarette products: correlation to liquid composition and design characteristics, *Nicotine & Tobacco Research*, 2018, **20**, 215-223, doi: 10.1093/ntr/ntw280.

[8] K. Bekki, S. Uchiyama, K. Ohta, Y. Inaba, H. Nakagome, N. Kunugita, Carbonyl compounds generated from electronic cigarettes, *International Journal of Environmental Research and Public Health*, 2014, **11**, 11192-11200, doi: 10.3390/ijerph111111192.

[9] N. L. Benowitz, J. B. Fraiman, Cardiovascular effects of electronic cigarettes, *Nat. Rev. Cardiol.*, 2017, **14**, 447-456, doi: 10.1038/nrcardio.2017.36.

[10] G. Zhang, Z. Wang, K. Zhang, R. Hou, C. Xing, Q. Yu, E. Liu, Safety assessment of electronic cigarettes and their relationship with cardiovascular disease, *International Journal of Environmental Research and Public Health*, 2018, **15**, 75, doi: 10.3390/ijerph15010075.

[11] E. Díaz, M. E. Sad, E. Iglesia, Homogeneous oxidation reactions of propanediols at low temperatures, *ChemSusChem*, 2010, **3**, 1063-1070, doi: 10.1002/cssc.201000142.

[12] C. R. Ayre, R. J. Madix, The adsorption and reaction of 1, 2-propanediol on Ag(110) under oxygen lean conditions, *Surface Science*, 1994, **303**, 279-296, doi: 10.1016/0039-6028(94)90776-5.

[13] M. A. Salaev, O. K. Poleshchuk, O. V. Vodyankina, Propylene glycol oxidation over silver catalysts: a theoretical study, *Journal of Molecular Catalysis A: Chemical*, 2016, **417**, 36-42, doi: 10.1016/j.molcata.2016.03.011.

[14] P. Wang, W. Chen, J. Liao, T. Matsuo, K. Ito, J. Fowles, D. Shusterman, M. Mendell, K. Kumagai, A device-independent evaluation of carbonyl emissions from heated electronic cigarette solvents, *PLoS One*, 2017, **12**, e0169811, doi: 10.1371/journal.pone.0169811.

[15] N. A. Saliba, A. El Hellani, E. Honein, R. Salman, S. Talih, J. Zeaiter, A. Shihadeh, Surface chemistry of electronic cigarette electrical heating coils: effects of metal type on propylene glycol thermal decomposition, *Journal of Analytical and Applied Pyrolysis*, 2018, **134**, 520-525, doi: 10.1016/j.jaap.2018.07.019.

[16] "Formaldehyde and Cancer Risk," Natl. Cancer Inst. (2011).

[17] "Acetaldehyde: Hazard Summary," Environ. Prot. Agency (2016).

[18] "National Toxicology Program, 12th Report on Carcinogens," U.S. National Library of Medicine (2011).

[19] "Toxicological Review of Propionaldehyde," U.S. Environmental Protection Agency (2008).

[20] B. Urych, Determination of kinetic parameters of coal pyrolysis to simulate the process of underground coal gasification (UCG), *Journal of Sustainable Mining*, 2014, **13**, 3-9, doi: 10.7424/jsm140102.

[21] T. P. Senftle, S. Hong, M. M. Islam, S. B. Kylasa, Y. Zheng, Y. K. Shin, C. Junkermeier, R. Engel-Herbert, M. J. Janik, H. M. Aktulga, T. Verstraelen, A. Grama, A. C. T. van Duin, The ReaxFF reactive force-field: development, applications and future directions, *Npj Computational Materials*, 2016, **2**, 15011, doi: 10.1038/npjcompumats.2015.11.

[22] S. Talih, Z. Balhas, R. Salman, R. El-Hage, N. Karaoghlanian, A. El-Hellani, M. Baassiri, E. Jaroudi, T. Eissenberg, N. Saliba, A. Shihadeh, Transport phenomena governing nicotine emissions from electronic cigarettes: model formulation and experimental investigation, *Aerosol Science and Technology*, 2017, **51**, 1-11, doi: 10.1080/02786826.2016.1257853.

[23] M. Al Rashidi, A. Shihadeh, N. A. Saliba, Volatile aldehydes in the mainstream smoke of the narghile waterpipe, *Food and Chemical Toxicology*, 2008, **46**, 3546-3549, doi: 10.1016/j.fct.2008.09.007.

[24] "Reaxff User Manual," Software for Chemistry and Materials (2002).

[25] Reaxff: reactive md with graphical interface and analysis tools, https://www.scm.com/product/reaxff/.

[26] "Included force fields," Software for Chemistry and Materials (2021). https://www.scm.com/doc/ReaxFF/Included_Forcefields.html.

[27] Q.-D. Wang, J.-B. Wang, J.-Q. Li, N.-X. Tan, X.-Y. Li, Reactive molecular dynamics simulation and chemical kinetic modeling of pyrolysis and combustion of n-dodecane, *Combustion and Flame*, 2011, **158**, 217-226, doi:

10.1016/j.combustflame.2010.08.010.
[28] T. Zhao, T. Li, Z. Xin, L. Zou, L. Zhang, A ReaxFF-based molecular dynamics simulation of the pyrolysis mechanism for polycarbonate, *Energy & Fuels*, 2018, **32**, 2156-2162, doi: 10.1021/acs.energyfuels.7b03332.
[29] L. Martínez, R. Andrade, E. G. Birgin, J. M. Martínez, PACKMOL: A package for building initial configurations for molecular dynamics simulations, *Journal of Computational Chemistry*, 2009, **30**, 2157-2164, doi: 10.1002/jcc.21224.
[30] T. Morishita, Fluctuation formulas in molecular-dynamics simulations with the weak coupling heat bath, *The Journal of Chemical Physics*, 2000, **113**, 2976-2982, doi: 10.1063/1.1287333.
[31] S. Arvelos, O. AbrahãoJr, C. Eponina Hori, ReaxFF molecular dynamics study on the pyrolysis process of cyclohexanone, *Journal of Analytical and Applied Pyrolysis*, 2019, **141**, 104620, doi: 10.1016/j.jaap.2019.05.009.
[32] P. G. Shields, M. Berman, T. M. Brasky, J. L. Freudenheim, E. Mathe, J. P. McElroy, M.-A. Song, M. D. Wewers, A review of pulmonary toxicity of electronic cigarettes in the context of smoking: a focus on inflammation, *Cancer Epidemiology, Biomarkers & Prevention*, 2017, **26**, 1175-1191, doi: 10.1158/1055-9965.epi-17-0358.
[33] R. P. Jensen, R. M. Strongin, D. H. Peyton, Solvent chemistry in the electronic cigarette reaction vessel, *Scientific Reports*, 2017, **7**, 42549, doi: 10.1038/srep42549.
[34] A. S. Perlin, Glycol-cleavage oxidation, *Advances in Carbohydrate Chemistry and Biochemistry*, 2006, **60**, 183-250, doi: 10.1016/S0065-2318(06)60005-X.

Author Information

Christina AlGemayel *is a research assistant at the Aerosol Research Laboratory at the American University of Beirut (AUB) where she obtained her B.E. and M.E. in chemical engineering. Her research focuses on molecular dynamics, kinetic modeling, and analytical chemistry.*

Dr. Ahmad El Hellani *Assistant Professor in the Environmental Health Sciences, College of Public Health, The Ohio State University. He is an Organic/Analytical chemist that went from fundamental organometallic chemistry research to be interested in the assessment of human exposure to toxicants from various sources, especially tobacco products. He studies tobacco emissions in a controlled analytical lab setting using smoking machines, in a clinical lab setting using real-time sampling devices, and in a chamber lab setting for the assessment of secondhand emissions. His work is interdisciplinary by nature, and he is currently conducting clinical studies to assess tobacco product abuse liability and toxicity.*

Rola Salman *obtained her BS in Biochemistry from Lebanese University. She joined the Aerosol Research Lab in 2008 as a research scientist. Her research focuses on measuring toxicant yields from tobacco and non-tobacco products in waterpipe, conventional cigarette, and different designs of electronic cigarettes.*

Najat A. Saliba *is currently a member of the Parliament of the Lebanese Government. She is also a Professor in Chemistry at the American University of Beirut. Saliba leads several locally relevant and globally important projects related to understanding the chemistry of inhalable tobacco and non-tobacco smoke and atmospheric aerosols. She is the co-founder and executive director of Khaddit Beirut and the Director and founder of the Environment Academy (EA). In 2021, she was invited to serve as a Member of the Scientific Board of the International Basic Science Programme (IBSP) at UNESCO and as a Chair of a Technical Advisory Group on the Global Air Quality Platform and Health (GAPH-TAG) at WHO. She was also nominated by Apolitical's the 12 most influential people in climate justice and 100 most influential people in Gender Policy in 2021. She received the 2019 L'Oreal-UNESCO International Award for Women in Science, the National Order of the Cedar from the President of the Lebanese Republic, the Honorary Cedar Shield from the Speaker of the Parliament of Lebanon and the Paul Harris Fellow Pin from the Rotary Club Beirut Cedars. Also, in 2019 she was voted among the top 100 most influential women by BBC. In 2016 she received the Lebanese National Council for Scientific Research Award in the Environmental Category.*

Alan Shihadeh *is Dean of the Maroun Semaan Faculty of Engineering and Architecture at the American University of Beirut (AUB). Shihadeh earned his undergraduate degree from the University of Texas at Austin and his doctorate in mechanical engineering at the Massachusetts Institute of Technology (MIT) in the field of combustion in 1998. He taught at Birzeit University as a Fulbright fellow before joining AUB as an assistant professor of mechanical engineering in 2000. Shihadeh is also Project Director at the Virginia Commonwealth University Center for the Study of Tobacco Products, founding director of the Aerosol Research Laboratory, and co-director of the Collaborative for the Study of Inhaled Atmospheric Aerosols (CARS).*

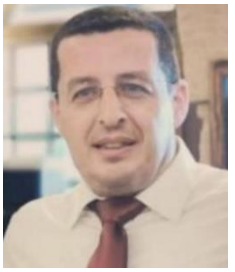

Dr. Joseph Zeaiter *received his PhD in Chemical Engineering (Process Systems Engineering) from the University of Sydney and joined the process industry, as an advanced process control /senior consultant working on projects in oil and gas, petrochemicals, power plants and mining. He is currently an associate professor in Chemical Engineering at the American University of Beirut (AUB) where his research interests are focused on catalytic pyro-gasification, hydrogen from natural gas conversion, and thermal solar energy for renewable fuel production.*